Macromolecules

ARTICLE

pubs.acs.org/Macromolecules

n-Type Conjugated Polyisoindigos

Romain Stalder,[†] Jianguo Mei,[†] Jegadesan Subbiah,[‡] Caroline Grand,[†] Leandro A. Estrada,[†] Franky So,[‡] and John R. Reynolds*[,†]

[†]The George and Josephine Butler Polymer Research Laboratory, Department of Chemistry, Center for Macromolecular Science and Engineering, and [‡]Department of Materials Science and Engineering, University of Florida, Gainesville, Florida 32611-7200, United States

Supporting Information

ABSTRACT: The conjugated electron acceptor isoindigo was used to synthesize two conjugated polymers with backbones composed exclusively of electron-deficient units. Suzuki polycondensation afforded the homopolymer of isoindigo and a copolymer with 2,1,3-benzothiadiazole as repeat unit. The materials are thermally stable up to 380 °C, along with being soluble in and processable from common organic solvents. The polymers absorb light broadly throughout the visible spectrum, with optical bandgaps of 1.70 and 1.77 eV, respectively. Both polymers reduce reversibly with LUMO energy levels at −3.84 and −3.90 eV for the homopolymer and the copolymer, respectively, close to the value of −4.10 eV found for fullerenes such as $PC_{60}BM$ when measured under identical conditions. The polymers HOMO levels were calculated at −5.54 and −5.67 eV, respectively, based on their optical band gaps. Spectroelectrochemical measurements on thin films of the homopolymer showed the generation of stable negative charge carriers, accompanied by colored-to-transmissive electrochromism in the films upon reduction. The n-type character of these polymers motivated the fabrication of all-polymer solar cells using blends of poly(3-hexylthiophene) and the homopolymer of isoindigo, yielding efficiencies approaching 0.5%, with room for optimization based on the observed surface morphology of the blend films.

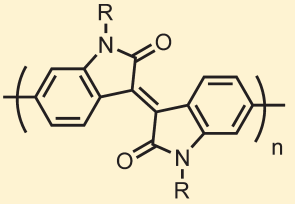

Poly(il)

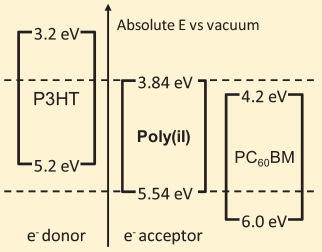

INTRODUCTION

The field of organic electronics relies on the design of increasingly high performance conjugated materials as active layer components in organic photovoltaics (OPVs), field-effect transistors (OFETs), light-emitting diodes, or electrochromics. Each material differs in its ability to balance hole (p-type) and electron (n-type) carrier creation and transport in devices, which depends on the energy level of its frontier molecular orbitals and its ability to adopt a suitable morphology for charge carrier transport. The latter is closely related to the molecular weight and the polydispersity of the material, ranging from well-defined discrete oligomers to linear fully conjugated polymers. While the majority of conjugated materials for all-organic electronics developed up to date are p-type, their n-type counterparts are equally attractive.[1−4] To date, most of the highest impact n-type conjugated materials reported recently have a (hetero)aromatic core bearing either fluorocarbon substituents[5−8] or imide electron-withdrawing groups. Homo- or copolymers of diketopyrrolopyrrole[9] (DPP), benzobisimidazobenzophenanthroline[10−12] (BBL), perylene diimide[13−15] (PDI), naphthalene diimide[13,16−18] (NDI), bithiophene imide[19,20] (BTI), and bisindenofluorene[21] have been reported as high electron mobility materials, some exceeding 0.1 $cm^2\ V^{-1}\ s^{-1}$ in air-stable OFETs. These materials should have high electron affinities (deep LUMOs) in order to sustain an energy barrier to ambient chemical oxidation of negatively charged carriers generated upon n-type doping.[22]

Low bandgap n-type conjugated polymers with high electron affinities and high ionization potentials (ambient stable) can play an important role in the related field of all-polymer solar cells because the commonly used fullerene derivatives typically have limited light absorption in the visible region. So far, the steady development of organic solar cells based on bulk heterojunctions (BHJs) has proven promising, especially in devices composed of p-type conjugated polymers and n-type fullerenes derivatives which now exceed 7% efficiency under AM 1.5 illumination.[23−26] Fullerene derivatives, such as $PC_{60}BM$ and $PC_{70}BM$, are constant components in the highest efficiency cells due to their advantageous electron mobility and their ability to crystallize into charge percolation networks.[27−32] The main disadvantage of fullerenes for BHJ cells is the limited chemical modifications available to extend their light absorption to wavelengths longer than 600 nm,[33−35] explaining the extensive synthetic effort focusing rather on broadening the spectral absorption of their donor−acceptor (D−A) p-type polymer counterparts.[36,37] As an alternative approach, molecular surrogates of fullerenes such as PDIs,[38,39] bifluorenylidene,[40] malononitriles,[41,42] or dicyanoimidazoles (vinazenes)[43,44] have been recently explored.[45] Soluble n-type polymers are also attractive because of their versatile processability: their macromolecular nature yields high-quality thin films as active layers, while variations in the side-chain can control the material's solubility and phase separation in the bulk.

Received: June 7, 2011
Revised: June 27, 2011
Published: July 29, 2011

In all-polymer solar cells, properties specific to polymer/polymer blends can influence the morphology in processed films.[46,47] Successfully performed for fullerene or other n-type small molecule based BHJs, the use of solvent mixtures to process polymer/polymer blends along with various film treatments (e.g., solvent vapor annealing or thermal annealing) can yield the desired phase segregation scales in the active layer.[48−50] The interaction parameters of each polymer with its counterpart, the device substrate, or the ambient vapor can lead to a favorable vertical segregation of the p- and n-type polymer within the active layer.[51−53] Except for BBL-based devices,[54,55] palladium-catalyzed cross-couplings are used to synthesize n-type D−A polymers for most all-polymer solar cells incorporating cyanovinylenes,[56−58] PDIs,[15,50,59,60] or 2,1,3-benzothiadiazole[61,62] (BTD) acceptors in conjugation with various donors, yielding maximum efficiencies to date between 1.8% and 2.3% at AM 1.5.

In all-polymer solar cells, the n-type material is a polymer which should fulfill specific energy levels requirements with respect to the p-type polymer in the active layer.[46,61] The most common p-type material used in all-polymer OPVs are derivatives of alkylated poly(thiophenes) and poly(phenylenevinylenes), which have HOMO and LUMO levels in the −5.2 to −5.4 eV and −3.1 to −3.2 eV ranges, respectively.[63] The n-type polymer used in heterojunction with such p-type polymers should thus be designed with HOMO and LUMO levels lower than −5.5 to −5.7 eV and −3.4 to −3.5 eV, respectively, to achieve energy levels offsets greater than 0.3 eV which will drive the excitons to the charge-separated state at the p/n-type interface. To be able to compete with the current fullerene derivatives, the scale of the energy offsets for the n-type polymer should be balanced with a bandgap below 1.8 eV to extend its absorption into the near-IR.

Our group introduced isoindigo (iI) as a novel acceptor in D−A conjugated p-type molecules[64] and polymers.[65] Our preliminary results on molecular solar cells[64] prompted us to systematically study the correlation between donor substituent and iI-based polymer absorption spectrum. It was found that the LUMO is localized in the iI units which permits tuning of the HOMO levels via manipulation of the donor counterparts.[65] Following on this, new D−A polymers based on isoindigo have been used by others as components of solar cells, memory devices, and air-stable OFETs.[66−70] These D−A polymers have been used as p-type components in conjunction with fullerenes in solar cells reaching 3.0% efficiency.[67,68,70] Combining voltammetry and UV−vis−NIR spectroscopy, all reported materials with LUMO energies in the −3.7 to −4.0 eV range and tunable deep HOMO energies between −5.5 and −5.9 eV depending on the nature of the electron-rich unit conjugated with isoindigo. With optical bandgaps reported between 1.6 and 1.9 eV, these polymers exhibit tunable broad absorption to wavelengths longer than 750 nm. Isoindigo D−A polymers can also exhibit high hole mobilities, with a recent report of air-stable p-type OFETs based on the isoindigo-*co*-bithiophene repeat unit, reaching mobilities up to 0.79 $cm^2\ V^{-1}\ s^{-1}$.[66]

Motivated by such low-lying energy levels and extended light absorption, we report herein on two new isoindigo-based conjugated polymers with backbones *exclusively composed of electron-deficient units*. In contrast to the more common donor−acceptor approach widely used to synthesize n-type conjugated polymers, the versatile chemistry of isoindigo allowed us to synthesize two soluble high molecular weight all-acceptor polymers: a homopolymer of isoindigo, **Poly(iI)**, and a copolymer of isoindigo with 2,1,3-benzothiadiazole alternating in the repeat unit, **Poly(iI-BTD)**. These two polymers absorb broadly in the visible region with the more red-shifted **Poly(iI)** absorbing up to 730 nm and possess optical bandgaps below 1.8 eV. DFT calculations allowed us to map their molecular orbitals and better understand their optical properties on the basis of electronic effects. The energy levels measured by reductive differential pulse voltammetry (DPV) are located between −3.8 and −3.9 eV. We deduced the HOMO levels from the optical bandgaps to be below −5.5 eV. Given the stability and reversibility of the reduction of **Poly(iI)**, we conducted spectroelectrochemistry experiments on thin films to confirm the ability of this polymer to accept and stabilize electrons. We observed repeatable colored-to-transmissive electrochromism upon reduction of the **Poly(iI)** films. Because **Poly(iI)** has suitable deep HOMO and LUMO levels and extended absorption to 730 nm, we investigated its use as an electron-acceptor in all-polymer solar cells in BHJ with P3HT. We show preliminary all-polymer solar cell power conversion efficiencies approaching 0.5% in 1:1 blends of **Poly(iI)** and P3HT, which could be optimized in future work by thorough device processing studies to achieve the desired phase separation. While, to the best of our knowledge, this is the first publication of **Poly(iI)** in the open scientific literature, its preparation has been discussed in a patent application.[71]

RESULTS AND DISCUSSION

Monomer and Polymer Synthesis. The most useful derivative of isoindigo for fully conjugated systems is 6,6′-dibromoisoindigo, which can be easily obtained from the condensation of 6-bromoisatin and 6-bromooxindole.[64] Typical yields for this acid-catalyzed condensation exceed 90%, which can be easily scaled up due to a straightforward purification: vacuum filtration followed by washing with ethanol and ethyl acetate afford the pure condensation product. For solubility purposes, this derivative is readily alkylated under basic conditions using potassium carbonate in anhydrous DMF. Branched dialkylated dibromoisoindigo has been the main precursor for all recently synthesized isoindigo-based compounds for organic electronic applications.[64−70] While 2-ethylhexyl groups provide sufficient solubility in D−A copolymers of isoindigo with alkylated donors, the solubility of *N,N*′-bis(2-ethylhexyl)isoindigo-based D−A copolymers with unalkylated donors is such that solution processing for device fabrication becomes impractical.[65,70] Indeed, our first attempts to synthesize the homopolymer of isoindigo using 2-ethylhexyl side chains resulted in a large amount of insoluble material which precipitated out of the reaction medium as soon as the polymerization was initiated. Consequently, we employed 2-hexyldecyl side chains in the synthesis of the all-acceptor polymers described here (Scheme 1).[68] Transformation of **1** under Miyaura borylation conditions furnished the key synthon **2** in 75% yield. Precipitation of the reaction mixture in methanol, followed by successive dissolution and reprecipitation in chloroform and methanol, respectively, afforded **2** in high purity.

Diborylated monomer **2** was then copolymerized with its dibrominated analogue **1** under Suzuki polycondensation conditions in degassed toluene at 85 °C, using $Pd_2(dba)_3$ and tri(*o*-tolyl)phosphine as catalytic system and a degassed 1 M tetraethylammonium hydroxide aqueous solution as boron-activating base. These highly efficient Suzuki cross-coupling conditions

Scheme 1. Synthesis of Diborylated Monomer 2 and Polymers Poly(iI) and Poly(iI-BTD)

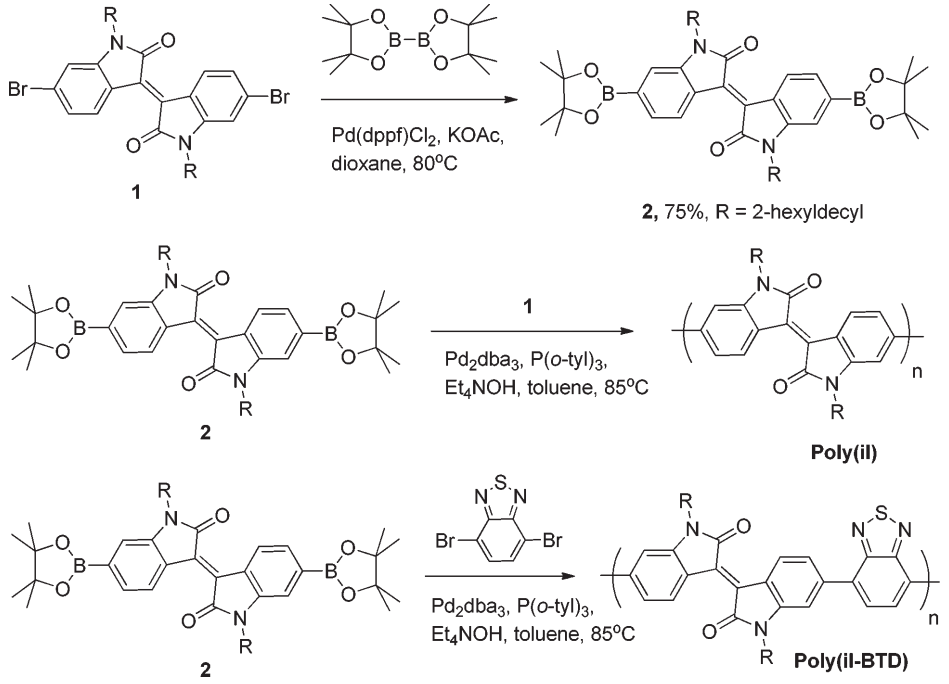

afforded the homopolymer of isoindigo, **Poly(iI)**, in excellent yield. The purification process involved precipitation into methanol, followed by Soxhlet extraction with methanol and then hexanes to remove low molecular weight product. A soluble higher molecular weight fraction of **Poly(iI)** was then extracted using chloroform, precipitated into methanol, and filtered, giving **Poly(iI)** in an overall yield of 74%. The number-average molecular weight of the chloroform soluble fraction of **Poly(iI)** is 28.7 kDa with a polydispersity index (PDI) of 2.4 as measured by size exclusion chromatography in THF against polystyrene standards. **Poly(iI)** is soluble in a range of common organic solvents, including tetrahydrofuran, toluene, dichloromethane, chloroform, and chlorinated benzenes. The ^{1}H NMR spectrum of the chloroform-soluble fraction shows broadened peaks in the aromatic region, between 8.8 and 9.1 ppm and 6.8−7.4 ppm, and a wide peak in the 3.6−4.3 ppm region with consistent integration corresponding to the methylene proton on the tertiary carbon of the 2-hexyldecyl side chains (Figure S2, Supporting Information). These chemical shifts are consistent with the repeat unit structure of **Poly(iI)**, further confirmed by elemental analysis.

By copolymerizing the diborylated isoindigo **2** with 4,7-dibromo-2,1,3-benzothiadiazole (Scheme 1), an alternating copolymer **Poly(iI-BTD)** was obtained. Similar high-yielding polymerization and purification procedures afforded **Poly(iI-BTD)** with an average molecular weight of 16.3 kDa and a PDI of 3.5 in 95% yield for the chloroform fraction after Soxhlet extraction. The solubility of **Poly(iI-BTD)** is similar to **Poly(iI)** using the same solvents. The remainder of the study was conducted on the materials extracted from chloroform during Soxhlet purification to ensure the highest average molecular weights available. The ^{1}H NMR spectrum of **Poly(iI-BTD)** features the same broad peaks in the aromatic region as the homopolymer. Additional peaks were observed near 9.4 ppm for **Poly(iI-BTD)** corresponding to the protons on the BTD ring (Figure S3). We employed thermogravimetric analysis (TGA) under nitrogen flow to evaluate the thermal stability of the purified polymers. Setting a 5% weight loss as the threshold for thermal decomposition, the polymers were both thermally stable up to 380 °C.

Optical Properties. We recorded the UV−vis absorption spectra of **Poly(iI)** and **Poly(iI-BTD)** in solution and in the solid state. As displayed in Figure 1, the UV−vis spectra of the polymer thin films on ITO-coated glass show broad absorption in the visible region. For the combined optical and electrochemical studies, the thin films were sprayed from a toluene solution rather than spin-cast to allow for more porous films in which counterions can penetrate more easily. **Poly(iI)** absorbs light at wavelengths longer than 700 nm, with λ_{max} at 690 nm and a low-energy onset of absorption at 731 nm. Of the two main absorption bands in the 400−730 nm region, the low-energy absorption band centered at 690 nm for **Poly(iI)** is more intense than its high-energy absorption band with a local maximum at 460 nm. Films of **Poly(iI)** have a blue-green color in the neutral state, as most of the red light is absorbed by the polymer. Thin films of **Poly(iI-BTD)** have a shorter λ_{max} at 464 nm, and while the low-energy absorption onset is at 700 nm, most of the light is absorbed between 400 and 600 nm. This trend holds in toluene solutions, with almost identical absorption profiles for the two polymers (Figure S8), suggesting little aggregation in the solid state without further film treatment after spray-coating. The measured molar absorptivities for **Poly(iI)** and **Poly(iI-BTD)** in toluene were 25 000 and 22 300 L mol^{-1} cm^{-1}, respectively, at their λ_{max}. From the low-energy onsets of the thin film absorption, solid-state optical bandgaps of 1.70 and 1.77 eV were calculated for **Poly(iI)** and **Poly(iI-BTD)**, respectively.

Structurally, **Poly(iI)** and **Poly(iI-BTD)** differ from one another based on the identity of the acceptor conjugated with, and adjacent to, each isoindigo unit. Two parameters can account for the difference in absorption spectra: a change in the electron-accepting strength of the moiety neighboring isoindigo along the

dx.doi.org/10.1021/ma2012706 |*Macromolecules* 2011, 44, 6303–6310

backbone and a change in the dihedral angle between the isoindigo unit and its neighbor. On the basis of these considerations, selected oligomers of **iI** and **iI-BTD** were subjected to DFT calculations in order to gain an understanding of their electronic characteristics (**iI** dimer and tetramer, plus **iI-BTD** monomer and dimer; see Supporting Information). Geometry optimizations, carried out at the B3LYP/6-31G* level of theory, indicated dihedral angles of 34°−36° between both **iI-iI** and **iI-BTD** repeat units (see Table S1). It has been previously shown that, while there are differences between the absolute energy values from the Kohn−Sham (KS) orbitals and those measured experimentally using UV photoelectron spectroscopy (UPS), the energetic splittings are consistent in many organic systems.[72] We compared the KS frontier orbital energies of the dimers **iI-iI** and **iI-BTD** and found that inclusion of the BTD units decreases the energy of the HOMO while increasing that of the LUMO. This trend, which is consistent with the calculations on the tetrameric species **iI-iI-iI-iI** and **iI-BTD-iI-BTD** (see Supporting Information, Figure S9), results in increased HOMO−LUMO bandgaps and, finally, higher energy optical transitions for the mixed acceptor system. Additionally, by analyzing the optimized structures and frontier orbital isodensity distributions for each species, the HOMO is dominated by a stilbene-like structure while the LUMO is localized on the central (3,3′-bipyrrolidine)-2,2′-dione unit (see Figure S9). On the basis of this consideration, the isoindigo unit can be regarded as an aromatic core with an intrinsic D−A character.

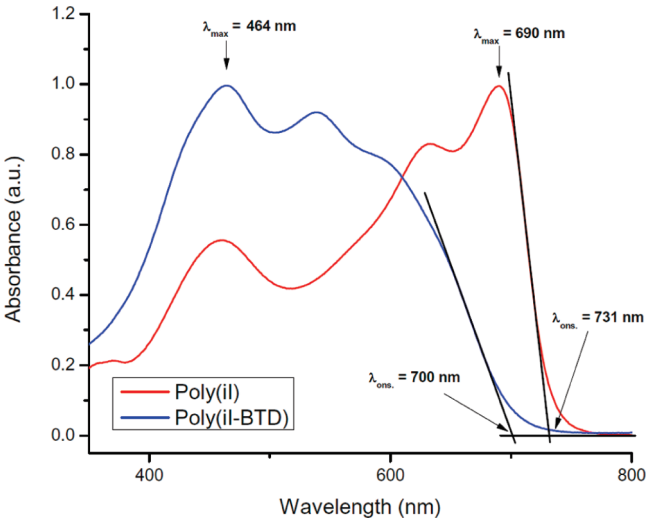

Figure 1. Normalized absorption profiles of **Poly(iI)** (red line) and **Poly(iI-BTD)** (blue line) thin films on ITO-coated glass.

Electrochemistry and Spectroelectrochemistry. In order to experimentally determine the energy levels of the polymers and be able to compare them to that of soluble fullerenes, we investigated the electrochemistry of **Poly(iI)** and **Poly(iI-BTD)** as thin films drop-cast onto Pt button electrodes in a 0.1 M $TBAPF_6$−acetonitrile solution under an inert atmosphere. All potentials reported here are calibrated against Fc/Fc^+. Figure 2a shows the tenth CV cycles of the oxidation and reduction of **Poly(iI)** and the reductive DPV. The reductive CV of **Poly(iI)** thin films shows one reversible redox process with cathodic and anodic peak currents at −1.36 and −1.24 V, respectively, and a half-wave potential at −1.30 V. The half-wave potentials remained constant with scan rates ranging from 10 to 200 mV/s (see Figure S10). With an anodic peak to cathodic peak potential difference under 160 mV even at relatively high scan rates, these results indicate a stable and relatively reversible redox process. Since the energy of SCE is 4.7 eV vs vacuum, and Fc/Fc^+ is +0.380 V vs SCE,[73,74] we used a Fc/Fc^+ redox standard set at −5.1 eV versus vacuum, a value recently highlighted by Bazan and co-workers.[75] The measured DPV reduction onset at −1.26 V for **Poly(iI)** corresponds to a LUMO energy of −3.84 eV. This is close to the value measured for $PC_{60}BM$ which reduces at −1.00 V (−4.10 eV) electrochemically, using DPV under the same conditions, and is similar to the accepted solid state value of 4.2 eV.[63] We attempted to electrochemically oxidize **Poly(iI)**, but only an irreversible and unstable redox process with a peak potential at +1.40 V was observed (see Supporting Information, Figure S11). Since the poor oxidation of the polymer prevents a

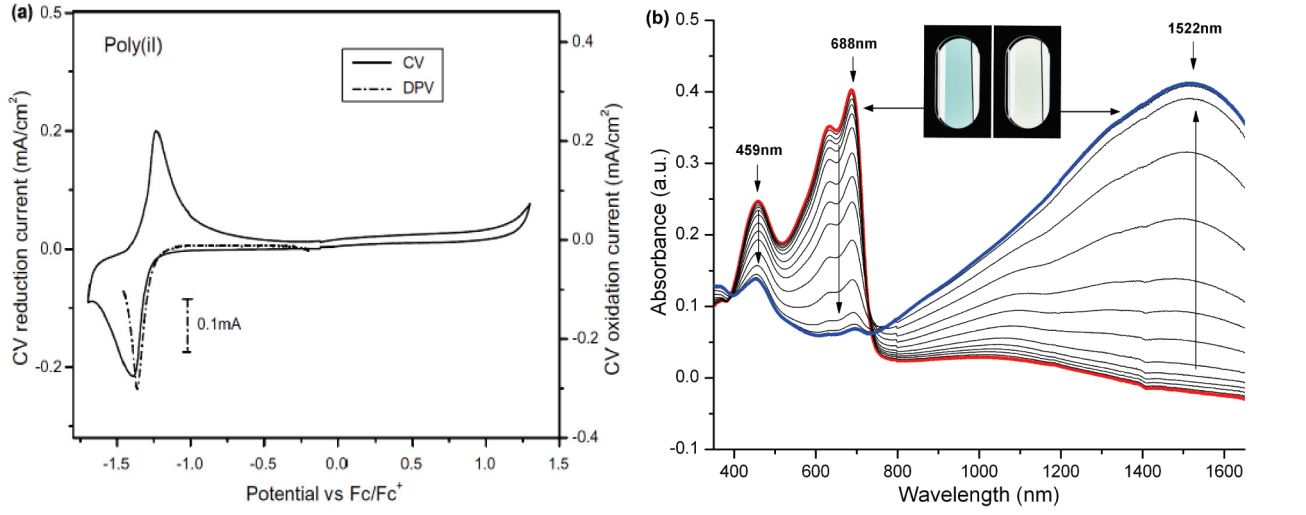

Figure 2. (a) Cyclic (solid line) and differential pulse (dashed line) voltammograms of **Poly(iI)** recorded from thin films on Pt-button electrodes, in 0.1 M $TBAPF_6$/acetonitrile electrolyte versus the Fc/Fc^+ redox standard. (b) Spectroelectrochemistry of **Poly(iI)** sprayed onto an ITO-coated glass slide. The film was subjected to 20 mV potential increments (first five spectra) and then 10 mV increments (last nine spectra) from −1.26 to −1.45 V vs Fc/Fc^+ in a 0.1 M $TEABF_4$/propylene carbonate electrolyte.

viable electrochemical calculation of the HOMO energy level, we deduced it from the optical bandgap of the thin films: for an optical bandgap of 1.70 eV, the corresponding HOMO energy level is at −5.54 eV.

We conducted similar voltammetry experiments on thin films of **Poly(iI-BTD)** drop-cast onto Pt button electrodes. At a scan rate of 50 mV/s, the reduction voltammetry shows one cathodic peak at −1.47 V and two anodic peaks upon reduction centered at −1.42 and −1.21 V (Figure S12). Only one cathodic peak was observed even after extending the potential range to −2.0 V. While the half-wave potentials remained constant at −1.31 V when the scan rate was increased from 10 to 200 mV/s, the peak-to-peak potential difference widened from 170 to 610 mV. This indicates that the reduction of **Poly(iI-BTD)** is less reversible than that of **Poly(iI)**. From the reductive DPV, an onset of reduction was measured at −1.20 V corresponding to a LUMO energy of −3.90 eV (Figure S12). In a similar way to **Poly(iI)**, the oxidation process is irreversible and unstable with currents steadily decreasing with successive recording cycles (see Figure S11). The solid state optical bandgap of 1.77 eV is equivalent to a HOMO energy of −5.67 eV.

Spectroelectrochemistry provides insight into the nature of the charged species generated along the conjugated backbone during the solid-state reduction process. To investigate the spectroelectrochemical behavior of **Poly(iI)**, we sprayed a toluene solution of the polymer onto ITO-coated glass slides, which serve as transmissive working electrodes. We selected tetraethylammonium tetrafluoroborate in propylene carbonate ($TEABF_4$/PC) as the supporting electrolyte for the reduction of the polymer films on ITO, since the redox processes proved to be more stable than when the $TBAPF_6$/ACN electrolyte was used. Figure 2b depicts the spectral changes upon application of successive step potentials from −1.26 to −1.45 V, with 10 mV potential increments for a **Poly(iI)** film on ITO. This small voltage difference to attain full reduction from the neutral polymer suggests a narrow distribution of states and that each species being reduced is chemically similar. No spectral change was observed when the potential was swept negative of 0 V up to −1.20 V: the red line in Figure 2b with peak absorption at 688 nm in the neutral film remained steady until potentials close to −1.25 V were reached. Within 0.19 V of further reduction from −1.26 to −1.45 V, the absorption bands at 459 and 688 nm of the neutral film decreased steadily to an almost complete bleaching of the absorption in the visible region. Concomitantly, a well-defined absorption band centered at 1522 nm emerged stabilizing in intensity at −1.45 V (blue line). While blue-green in the neutral state the polymer film cathodically bleaches at −1.45 V, as displayed in the inset pictures of Figure 2b, with a well-defined isosbestic point at 740 nm. We evaluated the color of the polymer films in the undoped and the reduced states as the human eye perceives them by measuring their $L^*a^*b^*$ values (CIE 1976 $L^*a^*b^*$ color space).[76] The neutral film shown in Figure 2b with a maximum absorbance of 0.4 at 688 nm has a low optical density with a^* and b^* values of −16 and −4, respectively. These values confirm a green to blue-green color of the undoped polymer, which is consistent with the trough observed in its neutral UV−vis spectrum at 520 nm and the lower relative intensity of the band at 459 nm with respect to the one at 688 nm. In the reduced state, the a^* and b^* values of the polymer film are respectively 1 and 6, confirming a transmissive doped state with a slight yellow hue, as expected from the small remnant absorption band at 459 nm at −1.45 V. Aside from dioxythiophene−cyanovinylene-based copolymers,[77,78] and to the best of our knowledge, this is the only example of a stable colored to transmissive electrochromic polymer upon n-doping (i.e., anodically coloring material, switching from a stable transmissive reduced state to a stable colored neutral state).[79]

The electrochemical experiments show a pronounced difference between the stable, reversible reduction processes compared to the unstable, irreversible oxidation processes, under the same electrochemical setup. In particular, the spectroelectrochemistry of **Poly(iI)** demonstrates the generation of stable negative charge carriers, an indication of the n-type character of all-acceptor polyisoindigos. While more quantitative experiments need to be performed to determine the exact nature of the charged species (i.e., radical anion or dianion), the excellent reversibility of the reduction points toward a single-electron process which yields a radical anion on the repeat unit of isoindigo for the absorption band in the near-IR centered at 1522 nm for the doped film.

All-Polymer Solar Cells. The electrochemistry results confirmed our expectations of high electron affinities (deep LUMOs) and high ionization potentials (deep HOMOs) for electron-deficient polyisoindigos. Figure 3a depicts where the energy levels of **Poly(iI)** lie with respect of that of P3HT (electron donor) and $PC_{60}BM$ (electron acceptor). Particularly, the electron affinity of **Poly(iI)** of −3.9 eV approaches that of the commonly used $PC_{60}BM$ set at −4.2 eV,[63] while the ionization potential of **Poly(iI)** of −5.6 eV is sufficiently high to drive exciton separation in BHJ cells with an appropriately chosen donor material. Having a bandgap below 1.8 eV allows for extended absorption throughout the visible spectrum—validating the candidacy of **Poly(iI)** as electron-accepting material for all-polymer solar cells. We selected P3HT as the p-type counterpart to **Poly(iI)** for all-polymer solar cells, since P3HT is a well-characterized polymer with HOMO and LUMO energy levels of −5.2 and −3.2 eV, respectively.[63] As shown in Figure 3a, this enables energy offsets greater than 0.3 eV between the HOMO (LUMO) of P3HT and **Poly(iI)**; the latter has a complementary absorption to P3HT, extending the absorption of the resulting blend by almost 100 nm into the near-IR in thin films (see Figure S14).

Bulk heterojunction photovoltaic cells were fabricated using P3HT as the donor and **Poly(iI)** as the acceptor. The polymers were dissolved separately in chlorobenzene under an inert atmosphere, and from the stock solutions, blends of 2:1, 1:1, and 1:2 P3HT:**Poly(iI)** were spin-cast onto patterned ITO slides. A schematic diagram of all-polymer cell with conventional device architecture is shown in the Supporting Information (Figure S13), along with the blend films absorptions for each ratio. It is important to note the level of contribution of **Poly(iI)** in the overall film absorption for the 2:1 P3HT:**Poly(iI)**, which is expected at such a ratio. At 1:2 P3HT:**Poly(iI)** blend, the absorption band at 688 nm from the contribution of **Poly(iI)** scales to ∼68% of the maximum absorption of P3HT. The photo $J-V$ characteristics of the devices made with three different P3HT:**Poly(iI)** weight ratios of 2:1, 1:1, and 1:2 as the active layer are shown in Figure 3b and the photovoltaic parameters (short-circuit current (J_{sc}), open-circuit voltage (V_{oc}), fill factor (FF), and power conversion efficiency (PCE)) of these devices are summarized in the inset.

The P3HT:**Poly(iI)** weight ratio of 1:1 showed the best device performance with a V_{oc} value of 0.62 V, a FF of 41%, and a J_{sc} value of 1.91 mA cm^{-2}, resulting in a PCE value of 0.47%.

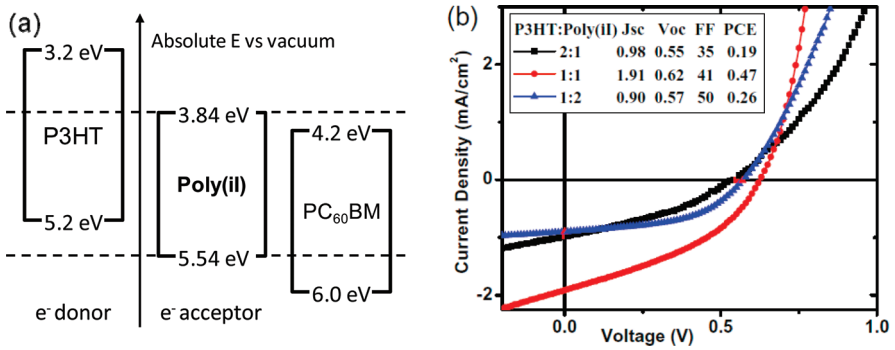

Figure 3. (a) Band structure diagram comparing the HOMO and LUMO levels of **Poly(iI)** and $PC_{60}BM$ and their offsets relative to the electron-donor P3HT. (b) $J-V$ curves of the P3HT:**Poly(iI)**-based BHJ solar cells with various blend ratios under AM 1.5 solar illumination, 100 mW cm^{-2}, in conventional solar cell architecture. Photovoltaic parameters are given in the inset: J_{sc} in mA cm^{-2}; V_{oc} in V; FF and PCE in %.

We denote an increasing fill factor of the devices with increasing **Poly(iI)** content, which reaches a maximum value of 50% when the blend ratio is 1:2. Meanwhile, increasing the **Poly(iI)** content in the blend ratio from 1:1 to 1:2 decreases the J_{sc}, lowering the overall device performance. We used AFM to probe the surface morphology of the active layer at different blend ratios (see Figure S15). While there is no significant difference in the feature sizes for the different blends, the scale of the phase-segregated regions is closer to the hundreds of nanometers rather than the 10−20 nm more suitable for efficient exciton dissociation to occur. The external quantum efficiency (EQE) of the P3HT:**Poly(iI)** device with the blend ratio of 1:1 is shown in Figure S14. The EQE measurements showed that the best polyisoindigo-based device exhibited broad photoresponse ranging from 350 to 750 nm with a maximum EQE of 12% at 520 nm.

The maximum PCE of 0.47% obtained for our polyisoindigo-based all-polymer solar cells is to put in perspective of the best all-polymer solar cells efficiency of 2.2−2.3% reported so far for BHJ devices.[50] Our preliminary solar cell results are encouraging since a more involved device fabrication study focusing on controlling the phase segregation scale should in time increase the short-circuit currents. Careful analysis of the charge carrier mobilities in pristine and blend films would give valuable information on the potential of polyisoindigos as n-type materials. Our first attempts yield electron mobilities in pristine films of **Poly(iI)** of 3.7×10^{-7} cm^2 V^{-1} s^{-1} on average, in an electron-only device based on a vertical architecture Al/**Poly(iI)**/LiF/Al, in the space charge limited current regime.

CONCLUSION

We synthesized two soluble all-acceptor conjugated polyisoindigos via Suzuki polycondensation. The polymers absorb broadly throughout the visible, up to 730 nm for the homopolymer of isoindigo. Its absorption profile is such that thin films of the homopolymer have a blue-green hue in the neutral state, and as the reduction electrochemistry of thin films is stable and reversible, we were able to reduce the polymer to a transmissive negatively charged state, spectroelectrochemistry confirming the generation of stable negative charge carriers in the film. This opens up a route for the development of scarcely available cathodically bleaching (anodically coloring) conjugated electrochromic polymers. The electrochemically confirmed n-type character of the homopolymer of isoindigo by design, combined with broad absorption and high electron affinities and ionization potentials, motivated the fabrication of all-polymer solar cells using blends of P3HT and polyisoindigo as active layer. Our promising preliminary results show that the power conversion efficiencies approaching 0.5% can likely be increased through a detailed study of device processing conditions using suitable solvent mixtures and post-fabrication treatments, as future work will focus on accessing proper BHJ film morphologies.

ASSOCIATED CONTENT

Supporting Information. Synthetic procedures and characterizations, materials and instrumentation details, TGA curves, DFT calculation details, cyclic voltammograms, differential pulse voltammograms, device fabrication details, blend films absorption and AFM images. This material is available free of charge via the Internet at http://pubs.acs.org.

AUTHOR INFORMATION

Corresponding Author
*E-mail: reynolds@chem.ufl.edu.

ACKNOWLEDGMENT

We gratefully acknowledge AFSOR (FA9550-09-1-0320) and the Office of Naval Research (N00014-11-1-0245) for financial support. R.S. acknowledges the University Alumni Awards Program for a fellowship. L.E. acknowledges the University of Florida High Performance Computing Center for providing computational resources for our DFT calculations.

REFERENCES

(1) Facchetti, A. *Chem. Mater.* **2011**, *23*, 733–758.
(2) Kulkarni, A. P.; Tonzola, C. J.; Babel, A.; Jenekhe, S. A. *Chem. Mater.* **2004**, *16*, 4556–4573.
(3) Wen, Y.; Liu, Y. *Adv. Mater.* **2010**, *22*, 1331–1345.
(4) Zhao, X.; Zhan, X. *Chem. Soc. Rev.* **2011**, *40*, 3728–3743.
(5) Facchetti, A.; Deng, Y.; Wang, A.; Koide, Y.; Sirringhaus, H.; Marks, T. J.; Friend, R. H. *Angew. Chem., Int. Ed.* **2000**, *39*, 4547–4551.
(6) Letizia, J. A.; Facchetti, A.; Stern, C. L.; Ratner, M. A.; Marks, T. J. *J. Am. Chem. Soc.* **2005**, *127*, 13476–13477.
(7) Tang, M. L.; Bao, Z. *Chem. Mater.* **2011**, *23*, 446–455.
(8) Yoon, M.-H.; DiBenedetto, S. A.; Facchetti, A.; Marks, T. J. *J. Am. Chem. Soc.* **2005**, *127*, 1348–1349.
(9) Cho, S.; Lee, J.; Tong, M.; Seo, J. H.; Yang, C. *Adv. Funct. Mater.* **2011**, *21*, 1910–1916.

(10) Babel, A.; Jenekhe, S. A. *Adv. Mater.* **2002**, *14*, 371–374.
(11) Babel, A.; Jenekhe, S. A. *J. Am. Chem. Soc.* **2003**, *125*, 13656–13657.
(12) Briseno, A. L.; Mannsfeld, S. C. B.; Shamberger, P. J.; Ohuchi, F. S.; Bao, Z.; Jenekhe, S. A.; Xia, Y. *Chem. Mater.* **2008**, *20*, 4712–4719.
(13) Chen, Z. H.; Zheng, Y.; Yan, H.; Facchetti, A. *J. Am. Chem. Soc.* **2009**, *131*, 8–9.
(14) Huang, C.; Barlow, S.; Marder, S. R. *J. Org. Chem.* **2011**, *76*, 2386–2407.
(15) Zhan, X.; Tan, Z. A.; Domercq, B.; An, Z.; Zhang, X.; Barlow, S.; Li, Y.; Zhu, D.; Kippelen, B.; Marder, S. R. *J. Am. Chem. Soc.* **2007**, *129*, 7246–7247.
(16) Guo, X.; Watson, M. D. *Org. Lett.* **2008**, *10*, 5333–5336.
(17) Kim, F. S.; Guo, X.; Watson, M. D.; Jenekhe, S. A. *Adv. Mater.* **2010**, *22*, 478–482.
(18) Yan, H.; Chen, Z.; Zheng, Y.; Newman, C.; Quinn, J. R.; Dotz, F.; Kastler, M.; Facchetti, A. *Nature* **2009**, *457*, 679–686.
(19) Guo, X.; Ortiz, R. P.; Zheng, Y.; Hu, Y.; Noh, Y.-Y.; Baeg, K.-J.; Facchetti, A.; Marks, T. J. *J. Am. Chem. Soc.* **2011**, *133*, 1405–1418.
(20) Letizia, J. A.; Salata, M. R.; Tribout, C. M.; Facchetti, A.; Ratner, M. A.; Marks, T. J. *J. Am. Chem. Soc.* **2008**, *130*, 9679–9694.
(21) Usta, H.; Risko, C.; Wang, Z.; Huang, H.; Deliomeroglu, M. K.; Zhukhovitskiy, A.; Facchetti, A.; Marks, T. J. *J. Am. Chem. Soc.* **2009**, *131*, 5586–5608.
(22) Anthopoulos, T., D.; Anyfantis, G. C.; Papavassiliou, G. C.; M. de Leeuw, D. *Appl. Phys. Lett.* **2007**, *90*, 122105.
(23) Chu, T.-Y.; Lu, J.; Beaupré, S.; Zhang, Y.; Pouliot, J.-R. M.; Wakim, S.; Zhou, J.; Leclerc, M.; Li, Z.; Ding, J.; Tao, Y. *J. Am. Chem. Soc.* **2011**, *133*, 4250–4253.
(24) Liang, Y.; Yu, L. *Acc. Chem. Res.* **2010**, *43*, 1227–1236.
(25) Price, S. C.; Stuart, A. C.; Yang, L.; Zhou, H.; You, W. *J. Am. Chem. Soc.* **2011**, *133*, 4625–4631.
(26) Amb, C. M.; Chen, S.; Graham, K. R.; Subbiah, J.; Small, C. E.; So, F.; Reynolds, J. R. *J. Am. Chem. Soc.* **2011**, *133*, 10062–10065.
(27) Cates, N. C.; Gysel, R.; Beiley, Z.; Miller, C. E.; Toney, M. F.; Heeney, M.; McCulloch, I.; McGehee, M. D. *Nano Lett.* **2009**, *9*, 4153–4157.
(28) Mihailetchi, V. D.; van Duren, J. K. J.; Blom, P. W. M.; Hummelen, J. C.; Janssen, R. A. J.; Kroon, J. M.; Rispens, M. T.; Verhees, W. J. H.; Wienk, M. M. *Adv. Funct. Mater.* **2003**, *13*, 43–46.
(29) Th, B. S.; Marjanovic, N.; Stadler, P.; Auinger, M.; Matt, G. J.; Gunes, S.; Sariciftci, N. S.; Schwodiauer, R.; Bauer, S. *J. Appl. Phys.* **2005**, *97*, 083714.
(30) Wienk, M., M.; Kroon, J. M.; Verhees, W. J. H.; Knol, J.; Hummelen, J. C.; van Hal, P., A.; Janssen, R., A. J. *Angew. Chem., Int. Ed.* **2003**, *42*, 3371–3375.
(31) Yang, X.; van Duren, J. K. J.; Rispens, M. T.; Hummelen, J. C.; Janssen, R. A. J.; Michels, M. A. J.; Loos, J. *Adv. Mater.* **2004**, *16*, 802–806.
(32) Yu, G.; Gao, J.; Hummelen, J. C.; Wudl, F.; Heeger, A. J. *Science* **1995**, *270*, 1789–1791.
(33) Mikroyannidis, J. A.; Kabanakis, A. N.; Sharma, S. S.; Sharma, G. D. *Adv. Funct. Mater.* **2011**, *21*, 746–755.
(34) Mikroyannidis, J. A.; Tsagkournos, D. V.; Sharma, S. S.; Sharma, G. D. *J. Phys. Chem. C* **2011**, *115*, 7806–7816.
(35) Varotto, A.; Treat, N. D.; Jo, J.; Shuttle, C. G.; Batara, N. A.; Brunetti, F. G.; Seo, J. H.; Chabinyc, M. L.; Hawker, C. J.; Heeger, A. J.; Wudl, F. *Angew. Chem., Int. Ed.* **2011**, *50*, 5166–5169.
(36) Chen, J. W.; Cao, Y. *Acc. Chem. Res.* **2009**, *42*, 1709–1718.
(37) Cheng, Y. J.; Yang, S. H.; Hsu, C. S. *Chem. Rev.* **2009**, *109*, 5868–5923.
(38) Rajaram, S.; Armstrong, P. B.; Kim, B. J.; Fréchet, J. M. J. *Chem. Mater.* **2009**, *21*, 1775–1777.
(39) Sharma, G. D.; Suresh, P.; Mikroyannidis, J. A.; Stylianakis, M. M. *J. Mater. Chem.* **2010**, *20*, 561–567.
(40) Brunetti, F. G.; Gong, X.; Tong, M.; Heeger, A. J.; Wudl, F. *Angew. Chem., Int. Ed.* **2010**, *49*, 532–536.
(41) Schwenn, P. E.; Gui, K.; Nardes, A. M.; Krueger, K. B.; Lee, K. H.; Mutkins, K.; Rubinstein-Dunlop, H.; Shaw, P. E.; Kopidakis, N.; Burn, P. L.; Meredith, P. *Adv. Energy Mater.* **2011**, *1*, 73–81.
(42) Zhou, Y.; Pei, J.; Dong, Q.; Sun, X.; Liu, Y.; Tian, W. *J. Phys. Chem. C* **2009**, *113*, 7882–7886.
(43) Shin, R. Y. C.; Kietzke, T.; Sudhakar, S.; Dodabalapur, A.; Chen, Z.-K.; Sellinger, A. *Chem. Mater.* **2007**, *19*, 1892–1894.
(44) Woo, C. H.; Holcombe, T. W.; Unruh, D. A.; Sellinger, A.; Fréchet, J. M. J. *Chem. Mater.* **2010**, *22*, 1673–1679.
(45) Anthony, J. E.; Facchetti, A.; Heeney, M.; Marder, S. R.; Zhan, X. *Adv. Mater.* **2010**, *22*, 3876–3892.
(46) McNeill, C. R.; Greenham, N. C. *Adv. Mater.* **2009**, *21*, 3840–3850.
(47) Veenstra, S., C.; Loos, J.; Kroon, J. M. *Prog. Photovolt.: Res. Appl.* **2007**, *15*, 727–740.
(48) Arias, A. C.; MacKenzie, J. D.; Stevenson, R.; Halls, J. J. M.; Inbasekaran, M.; Woo, E. P.; Richards, D.; Friend, R. H. *Macromolecules* **2001**, *34*, 6005–6013.
(49) Campbell, A. R.; Hodgkiss, J. M.; Westenhoff, S.; Howard, I. A.; Marsh, R. A.; McNeill, C. R.; Friend, R. H.; Greenham, N. C. *Nano Lett.* **2008**, *8*, 3942–3947.
(50) Zhou, E.; Cong, J.; Wei, Q.; Tajima, K.; Yang, C.; Hashimoto, K. *Angew. Chem., Int. Ed.* **2011**, *50*, 2799–2803.
(51) Arias, A. C.; Corcoran, N.; Banach, M.; Friend, R. H.; MacKenzie, J. D.; Huck, W. T. S. *App. Phys. Lett.* **2002**, *80*, 1695–1697.
(52) Chappell, J.; Lidzey, D. G.; Jukes, P. C.; Higgins, A. M.; Thompson, R. L.; O'Connor, S.; Grizzi, I.; Fletcher, R.; O'Brien, J.; Geoghegan, M.; Jones, R. A. L. *Nature Mater.* **2003**, *2*, 616–621.
(53) Kietzke, T.; Horhold, H.-H.; Neher, D. *Chem. Mater.* **2005**, *17*, 6532–6537.
(54) Alam, M. M.; Jenekhe, S. A. *Chem. Mater.* **2004**, *16*, 4647–4656.
(55) Jenekhe, S., A.; Yi, S. *Appl. Phys. Lett.* **2000**, *77*, 2635–2637.
(56) Granstrom, M.; Petritsch, K.; Arias, A. C.; Lux, A.; Andersson, M. R.; Friend, R. H. *Nature* **1998**, *395*, 257–260.
(57) Halls, J. J. M.; Walsh, C. A.; Greenham, N. C.; Marseglia, E. A.; Friend, R. H.; Moratti, S. C.; Holmes, A. B. *Nature* **1995**, *376*, 498–500.
(58) Holcombe, T. W.; Woo, C. H.; Kavulak, D. F. J.; Thompson, B. C.; Fréchet, J. M. J. *J. Am. Chem. Soc.* **2009**, *131*, 14160–14161.
(59) Tan, Z. a.; Zhou, E.; Zhan, X.; Wang, X.; Li, Y.; Barlow, S.; Marder, S. R. *Appl. Phys. Lett.* **2008**, *93*, 073309.
(60) Zhan, X. W.; Tan, Z. A.; Zhou, E. J.; Li, Y. F.; Misra, R.; Grant, A.; Domercq, B.; Zhang, X. H.; An, Z. S.; Zhang, X.; Barlow, S.; Kippelen, B.; Marder, S. R. *J. Mater. Chem.* **2009**, *19*, 5794–5803.
(61) Falzon, M.-F.; Wienk, M. M.; Janssen, R. A. J. *J. Phys. Chem. C* **2011**, *115*, 3178–3187.
(62) McNeill, C. R.; Abrusci, A.; Zaumseil, J.; Wilson, R.; McKiernan, M. J.; Burroughes, J. H.; Halls, J. J. M.; Greenham, N. C.; Friend, R. H. *Appl. Phys. Lett.* **2007**, *90*, 193506.
(63) Thompson, B. C.; Fréchet, J. M. J. *Angew. Chem., Int. Ed.* **2008**, *47*, 58–77.
(64) Mei, J.; Graham, K. R.; Stalder, R.; Reynolds, J. R. *Org. Lett.* **2010**, *12*, 660–663.
(65) Stalder, R.; Mei, J.; Reynolds, J. R. *Macromolecules* **2010**, *43*, 8348–8352.
(66) Lei, T.; Cao, Y.; Fan, Y.; Liu, C.-J.; Yuan, S.-C.; Pei, J. *J. Am. Chem. Soc.* **2011**, *133*, 6099–6101.
(67) Liu, B.; Zou, Y.; Peng, B.; Zhao, B.; Huang, K.; He, Y.; Pan, C. *Polym. Chem.* **2011**, *2*, 1156–1162.
(68) Wang, E.; Ma, Z.; Zhang, Z.; Henriksson, P.; Inganas, O.; Zhang, F.; Andersson, M. R. *Chem. Commun.* **2011**, *47*, 4908–4910.
(69) Xu, X.; Li, L.; Liu, B.; Zou, Y. *Appl. Phys. Lett.* **2011**, *98*, 063303–3.
(70) Zhang, G.; Fu, Y.; Xie, Z.; Zhang, Q. *Macromolecules* **2011**, *44*, 1414–1420.
(71) Flores, J.-C.; Berens, U.; Bienewald, F.; Kirner, H. J.; Turbiez, M. G. R. (CIBA) World Patent WO 2009/053291 A1, 2009.
(72) Lambert, C.; Risko, C.; Coropceanu, V.; Schelter, J. r.; Amthor, S.; Gruhn, N. E.; Durivage, J. C.; Brédas, J.-L. *J. Am. Chem. Soc.* **2005**, *127*, 8508–8516.
(73) Pavlishchuk, V. V.; Addison, A. W. *Inorg. Chim. Acta* **2000**, *298*, 97–102.

(74) Hansen, W. N.; Hansen, G. J. *Phys. Rev. A* **1987**, *36*, 1396–1402.
(75) Cardona, C. M.; Li, W.; Kaifer, A. E.; Stockdale, D.; Bazan, G. C. *Adv. Mater.* **2011**, *23*, 2367–2371.
(76) Dyer, A. L.; Thompson, E. J.; Reynolds, J. R. *ACS Appl. Mater. Interfaces* **2011**, *3*, 1787–1795.
(77) Galand, E. M.; Kim, Y.-G.; Mwaura, J. K.; Jones, A. G.; McCarley, T. D.; Shrotriya, V.; Yang, Y.; Reynolds, J. R. *Macromolecules* **2006**, *39*, 9132–9142.
(78) Thompson, B. C.; Kim, Y.-G.; McCarley, T. D.; Reynolds, J. R. *J. Am. Chem. Soc.* **2006**, *128*, 12714–12725.
(79) Beaujuge, P. M.; Reynolds, J. R. *Chem. Rev.* **2010**, *110*, 268–320.